This article has been accepted for inclusion in a future issue of this journal. Content is final as presented, with the exception of pagination.

Characterizing Background Signals and Noise in Spaceborne GNSS Reflection Ocean Observations

Scott Gleason, *Senior Member, IEEE*, Joel Johnson, *Fellow, IEEE*, Chris Ruf, *Fellow, IEEE*, and Charles Bussy-Virat

***Abstract*— This letter analyzes the background signals and thermal noise received over ocean scenes in spaceborne global navigation satellite system (GNSS)-reflectometry (GNSS-R) remote sensing using observations from the cyclone GNSS (CYGNSS) constellation. The measured noise floor contains a stable and predictable radiometric thermal noise component and a more variable background signal component from unintended specular reflections within the CYGNSS receive antenna pattern from all GNSS satellite constellations (GPS, Galileo, GLONASS, Beidou, and all SBAS). The presence of SBAS reflections, in particular, is evident in the noise floor measurements, especially the U.S. wide area augmentation system (WAAS) satellites. The results show that the impact is negligible, since background signal contributions by other GNSS transmitters affect both the "signal" and "noise" portions of CYGNSS's delay Doppler map measurements, and therefore cancel when the measured noise floor is subtracted from the desired signal. The potential increase in measurement uncertainty introduced by any residual background signal to the CYGNSS calibration is analyzed.**

***Index Terms*— Bistatic radar, calibration, cyclone global navigation satellite system (CYGNSS), global navigation satellite system (GNSS), GPS, noise, reflectometry, scatterometry.**

I. Introduction and Background

GLOBAL navigation satellite system (GNSS)-reflectometry (GNSS-R, [1]) performs earth remote sensing by measuring the bistatic reflections of signals transmitted from GNSS constellations (GPS, Galileo, GLONASS, and Satellite-Based Augmentation System SBAS). All the multiple satellites within a GNSS constellation typically transmit within the same frequency band but use spread spectrum techniques to distinguish the transmissions of different space vehicles [2].

This letter examines the contributions of all GNSS transmissions to the noise floor of a GNSS-R delay-Doppler map (DDM), using data from the on-orbit cyclone GNSS (CYGNSS) constellation [3]. The noise floor measured by CYGNSS is used in its Level 1 DDM calibration; errors in this measurement have the potential to affect the CYGNSS's estimates of surface-scattered power and subsequent ocean winds-peed retrievals [4].

On-orbit GNSS-R measurements both from CYGNSS and from the TechDemoSat (TDS)-1 satellite indicate that: 1) unintended signal reflections make up a significant component of the overall noise floor over the ocean and 2) they are stronger and more variable over ocean than land [5]. The results demonstrate that transmissions from other GNSS satellites (those not used to perform the GNSS-R remote sensing measurement) can significantly alter the observed noise.

II. Model of Cross Correlation Signal Power

An order of magnitude approximation for the background signal level added to the noise floor is developed using estimated high and low bounds of the transmit power for satellites, from the SBAS constellation. The noise counts, C_N, (unitless) obtained from GNSS-R measurement are linearly related to the observed noise floor by the receiver gain, G, such that

$$C_N = G P_{\text{total}} = G(P_o + P_{\text{xcorr}} + P_r + P_{\text{other}}) \tag{1}$$

where P_o is the noise power from upwelling earth thermal emission over the ocean, P_{xcorr} is the equivalent noise power of the correlation of the background signal from other GNSS transmitters, P_r is the receiver noise temperature, P_{other} is the noise from non-GNSS interference sources, $P_a = P_o + P_{\text{xcorr}} + P_{\text{other}}$ is the net noise power entering the antenna, and P_{total} is the total power in the measured noise floor. The level of the total cross correlation component, P_{xcorr}, is of concern if it is of sufficient magnitude to affect the received noise levels of processed measurements. Assuming that these contributions arise due to ocean-surface reflections, a simplified version of the bistatic radar equation [6] can be used to model the received power levels

$$P_{\text{xcorr}} = \sum_{n=1}^{N} \frac{P_{T,n} \lambda^2 \bar{G}_{T,n} \bar{\sigma}_{0,n} \bar{G}_{R,n} \bar{A}_n}{(4\pi)^3 (\bar{R}_{R,n})^2 (\bar{R}_{T,n})^2} \tag{2}$$

where $P_{T,n}$ and $G_{T,n}$ are the transmitter power and antenna gain for the nth source, $G_{R,n}$ is the receive antenna gain at the nth source specular reflection point, A_n is the corresponding

Manuscript received November 15, 2018; revised February 27, 2019 and May 7, 2019; accepted July 1, 2019. This work was supported by the NASA Cyclone GNSS (CyGNSS) Mission (NASA Earth Venture Program). *(Corresponding author: Scott Gleason.)*

S. Gleason is with the Constellation Observing System for Meteorology and Climate (COSMIC), University Corporation for Atmospheric Research,Boulder, CO 80307-3000 USA (e-mail: gleason@ucar.edu).

J. Johnson is with the Department of Electrical and Computer Engineering, Ohio State University, Columbus, OH 43212 USA.

C. Ruf is with the Department of Climate and Space Sciences and Engineering, University of Michigan, Ann Arbor, MI 48109-2143 USA.

C. Bussy-Virat is with the Department of Climate and Space Sciences and Engineering, University of Michigan, Ann Arbor, MI 48109 USA.

Color versions of one or more of the figures in this letter are available online at http://ieeexplore.ieee.org.

Digital Object Identifier 10.1109/LGRS.2019.2926695

1545-598X © 2019 IEEE. Personal use is permitted, but republication/redistribution requires IEEE permission.
See http://www.ieee.org/publications_standards/publications/rights/index.html for more information.

This article has been accepted for inclusion in a future issue of this journal. Content is final as presented, with the exception of pagination.

surface glistening zone area, and $R_{R,n}$ and $R_{T,n}$ are the associated nth specular point ranges for the receiver and the transmitter, respectively. The "bar" symbol over the variables indicates that these are approximate values resulting from a localized surface integration around the point of specular reflection.

Equation (2) makes clear that only GNSS transmitters having a specular point within the CYGNSS receive antenna pattern will make significant contributions. Section III considers specular points located over multiple CYGNSS orbits.

III. Model Predictions

A simulation was performed using the model described above to estimate the expected range of received power for the three SBAS wide area augmentation system (WAAS) satellites. As the actual transmit power, antenna patterns, and spacecraft attitudes are unknown, low and high bounds for the transmitter effective isotropic radiated power (EIRP) and surface reflectivity were sought. The limited analysis of the SBAS antennas and transmit powers reported in [7] shows that the WAAS satellites generally transmit at higher power levels than other SBAS constellations. For the purpose of estimating the cross correlation power, the following assumptions were made.

1) P_{ocean} is assumed roughly constant, or equivalently to vary more slowly in space than do fluctuations of P_{xcorr}.
2) The cross correlation rejection between the desired Pseudo Random Noise (PRN) code and other PRN codes is assumed to be ideal so that no coherent integration gain is added to the cross correlation power.
3) The transmitted EIRP ($P_{T,n}G_{T,n}$) is estimated to be between 28 dBW (approximate GPS satellite EIRP levels [8]) and 33 dBW; the upper limit was selected to increase the EIRP in proportion to the geosynchronous altitude of SBAS satellites.
4) The normalized bistatic radar cross section σ_0 values are 10 dB (low bound, high winds) and 20 dB (high bound, low winds); in reality, this will be a function of global surface wind speed, with lower winds resulting in higher values of σ_0.
5) The scattering area A was assumed to be 15 km $\times$ 15 km, based on the estimated glistening zone extent for a 30° incidence angle reflection for CYGNSS [6].
6) The receive antenna gain $G_{R,n}$ is estimated using a simulation of the CYGNSS satellite orbits and all resulting GNSS satellite reflection points within the CYGNSS receive antenna footprint. The pre-launch estimate of the CYGNSS Rx antenna pattern was used in the simulation.
7) Path losses $R_{R,n}$ and $R_{T,n}$ were estimated using the CYGNSS and GNSS transmitter orbit geometries. Typical values for these parameters, for a 30° incident reflection, are 580 and 48 600 km, respectively.

The simulation was run in 10 s time steps using CYGNSS spacecraft and GNSS orbits over two days, with only a short representative portion of the simulation shown in Fig. 1. The orbits were propagated using the SpOCK propagator developed at the University of Michigan [9]. The CYGNSS field of view (FOV) was determined by the pre-launch estimated science antenna patterns, while no FOV constraints were included for the WAAS satellites (as antenna and spacecraft attitude are not known). An example time series of predicted power levels for a typical triple WAAS reflection ($N = 3$) on both the starboard and port antennas is shown in Fig. 1. The "high power" case clearly results in power levels above the background ocean noise level (calculated assuming a 99-K ocean equivalent brightness temperature and a CYGNSS instrument bandwidth of 2 MHz) and Boltzmann's constant as $kT_B B_w$. This analysis is approximate but nevertheless illustrates that WAAS forward reflections can impact CYGNSS noise floor levels. Minimum and maximum predicted levels from the entire simulation are further summarized in Table I.

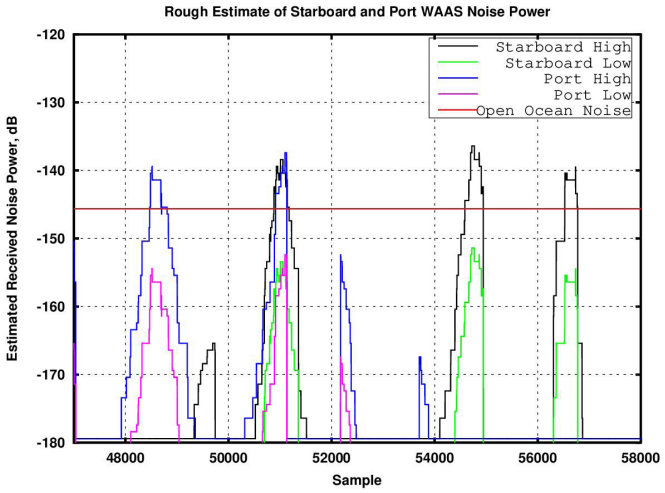


Fig. 1. Sample time series of estimated bistatic power from three WAAS satellites as received by a CYGNSS observatory. Calculated using the low and high transmit power and surface scattering assumptions listed in Table I.

IV. Observed CYGNSS Noise Floor Variations and Their Relationship to GNSS Constellations

The average noise floor of actual CYGNSS measurements was mapped globally to ascertain if its distribution exhibited coincidence with the coverage of WAAS and other GNSS constellations. The CYGNSS noise counts include contributions from the internal instrument noise and external noise captured by the antenna, with the sum of both multiplied by the total instrument gain, expressed as

$$C_N = G(P_r + P_a) = C_N^r + C_N^a \tag{3}$$

where P_r and P_a are the instrument and antenna noise power in watts, respectively. C_N^r and C_N^a are the instrument and antenna noise counts, respectively, and G is the total instrument processing gain.

In order to isolate the noise component received external to the antenna, it is necessary to correct for internal noise-level fluctuations caused by changing receiver temperatures. Internal instrument thermal noise counts can be estimated directly from the instrument calibration load temperature T_{cal}

$$C_N^r = GP_r = G(kT_{\text{cal}}B_W). \tag{4}$$

Here k is Boltzmann's constant, B_W is the processed signal bandwidth, and T_{cal} is the calibration load physical

This article has been accepted for inclusion in a future issue of this journal. Content is final as presented, with the exception of pagination.

TABLE I

MINIMUM AND MAXIMUM ESTIMATES OF RECEIVED CROSS CORRELATION POWER USING THE LISTED LOW AND HIGH BOUND ASSUMPTIONS FOR SOURCE EIRP AND SURFACE SCATTERING

Parameter	Low Assumption	High Assumption
GPS Transmit Power and Antenna Gain (EIRP) Assumption (dB)	28 dB	33 dB
σ_0 Assumption (dB)	10 dB	20 dB
Total P_{xcorr} Noise Power	-152 dBW	-136 dBW
Open Ocean (99 Kelvin) Reference Noise	-146 dBW	-146 dBW
Difference Between P_{xcorr} and Open Ocean Noise	6 dB below	10 dB above

temperature. Internal calibration load measurements are performed every 60 s providing an observation of the instrument noise counts, C_N^r, which includes instrument thermal noise fluctuations. With an estimate of C_N^r, it is possible to estimate the external antenna noise component in counts as

$$C_N^a = GP_a = G(P_o + P_{\text{xcorr}} + P_{\text{other}}) = C_N - C_N^r \quad (5)$$

where P_a is broken into several components, P_o is the ocean noise, P_{xcorr} is the noise due to cross correlation of other GNSS transmitters, and P_{other} is any additional non-GNSS noise or interference. With the variation in P_o assumed to be small and the effects of ground-based interference sources P_{other} rare, we are attempting to quantify the remaining term P_{xcorr}.

The resulting gridded and averaged external antenna noise levels C_N^a (in units watts, dBW) from all eight satellites over a 2-day period (June 7–8, 2018) are shown in Fig. 2. The results show clear geographic variations that are distinct for the port and starboard antennas. It is suspected that in addition to the effects of P_{xcorr} analyzed below, there are also probably non-GNSS high noise regions due to the presence of additional interfering signals, P_{other}, notably near the Middle East.

The WAAS satellites are in the geosynchronous orbit above the equator; the spatial distribution of the modeled WAAS received reflection power is shown in Fig. 3 as the sum of the CYGNSS satellite receive antenna gain for all three WAAS specular surface reflections. This is a measure of the total amount of CYGNSS antenna gain aimed at WAAS specular reflection points, each contributing additional noise to the CYGNSS observed noise floor. The total received antenna gain shown in Fig. 3 can be expressed as the sum of the CYGNSS receive antenna gain G_R for all three WAAS transmitters

$$G_R^{\text{SBAS}} = \sum_{n=1}^{M} G_R^n \quad (6)$$

where SBAS includes all the satellites in a given SBAS system of number M. Note that in the northern hemisphere, CYGNSS starboard antennas will generally be oriented southward, resulting in SBAS reflections in the starboard antenna. In the southern hemisphere, SBAS reflections appear more in the port antenna.

Although the CYGNSS noise distributions shown in Fig. 2 are different from the TDS noise distribution shown in Foti *et al.* [5], the results are consistent with the receive antenna gain patterns for both CYGNSS data and TDS. TDS carried a single nadir-oriented antenna (as opposed to the cross-track-oriented, north/south looking, CYGNSS antennas),

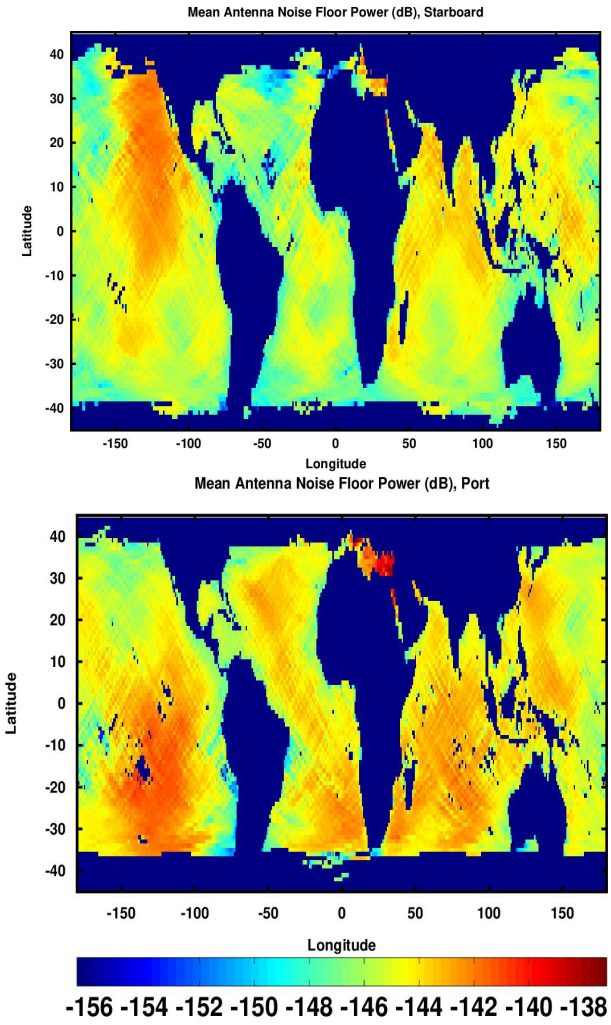


Fig. 2. (Top) Starboard and (bottom) port mean noise floor power (watts, dBW), two days of CYGNSS data (eight satellites).

which was more likely to view the SBAS power only near the equator, generally under the SBAS transmitters (where the specular reflection was captured in the main nadir antenna beam). Thus, we believe the receive antenna beam orientation and the specular reflection geometry with respect to the SBAS satellites explain the different spatial noise distributions between the CYGNSS and the TDS.

Fig. 4 shows mean CYGNSS noise levels, binned in intervals of 250 counts over the entire range of received noise levels versus the sum of the CYGNSS receive antenna gain (per (6) for the case of WAAS transmitters and similarly for

This article has been accepted for inclusion in a future issue of this journal. Content is final as presented, with the exception of pagination.

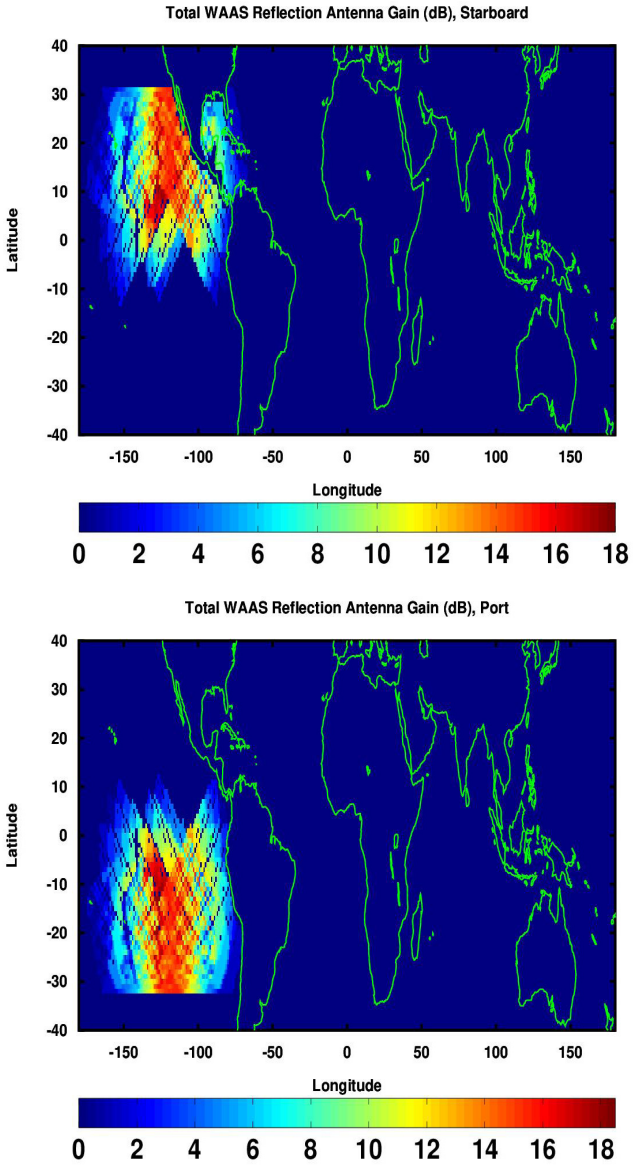


Fig. 3. (Top) Starboard and (bottom) port map of modeled WAAS specular reflection receiver gains (G_R^{WAAS}, dB) simulated over a two-day interval.

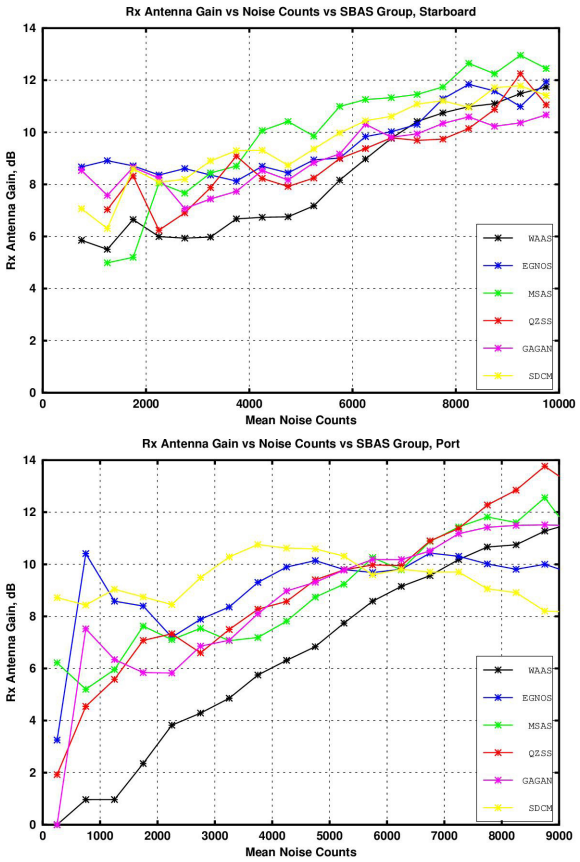


Fig. 4. (Top) Starboard and (bottom) port relationship between all SBAS constellation satellites (WAAS, European Geostationary Navigation Overlay Service (EGNOS), MTSAT Satellite Augmentation System (MSAS), Quasi Zenith Satellite System (QZSS), GPS Aided Geo Augmented Navigation System (GAGAN), System for Differential Corrections and Monitoring (SDCM)) total reflection antenna gain (G_R^{SBAS}) and CYGNSS noise floor counts.

other SBAS systems). These binned noise levels are plotted versus the summed CYGNSS receive antenna gain for all three WAAS specular points. This clearly shows that most SBAS systems contribute additional noise to the CYGNSS observed noise floors.

Similar correlation analyses were also performed for other GNSS constellations. Fig. 5 shows the resulting starboard and port noise floor levels versus the summed receive antenna gain for reflections from other GNSS constellations (for GPS, these include only satellites not being intentionally processed for the measurement). These results show the strongest evidence of correlation with the SBAS constellation and with other constellations (other GPS, Galileo, GLONASS, and Beidou) showing smaller or inconsistent trends.

The reason for the lack of a clear correlation between specular reflections of the non-SBAS constellation transmitters and CYGNSS noise levels is unknown. One possible explanation could be that the phasing of the GNSS satellites limits the number of additional specular reflections visible at one time in either of the two antenna surface footprints. In fact, it is unusual to have more than one additional non-selected specular reflection point in either antenna at any given time. Conversely, it is common for multiple additional SBAS satellites to be captured by the antenna at repeatable locations. More information on the CYGNSS spatial coverage and measurements tracks can be found in [3].

V. Impact on CYGNSS Calibration

The CYGNSS Level 1 Calibration algorithm [4] attempts to remove background signal and noise contributions to the portion of the DDM where the desired specular reflection signal resides. The algorithm assumes that those contributions are statistically the same in all portions of the DDM. DDM measurements are made at delay times prior to that of the desired reflected signal. The noise floor is estimated by averaging the DDM in the region of shorter delays above the surface. The resulting noise floor estimate is then subtracted from all pixels in the DDM to remove background contributions.

This article has been accepted for inclusion in a future issue of this journal. Content is final as presented, with the exception of pagination.

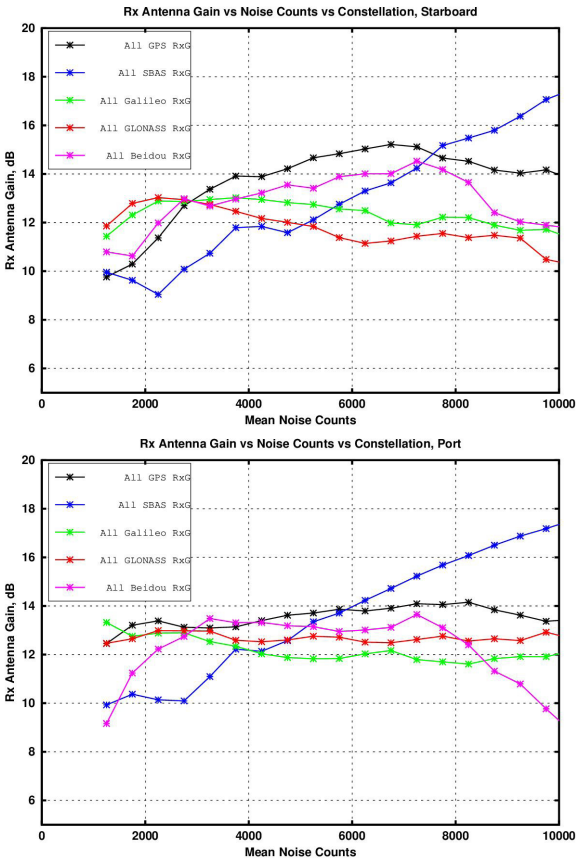


Fig. 5. (Top) Starboard and (bottom) port relationship between GPS, SBAS, Galileo, GLONASS, and Beidou GNSS constellation total reflection gain and CYGNSS noise floor.

We tested if it was reasonable to assume that cross correlation signal levels should be distributed uniformly throughout the DDM since the received signals are not synchronized in delay or Doppler with the desired PRN code. These contributions should, therefore, cancel near the signal delay portion of the DDM when the estimated noise floor is subtracted.

To assess the validity of this assumption, the consistency in the CYGNSS observed noise floor as a function of the delay was analyzed using a multi-hour collection of CYGNSS measurements in the CYGNSS's full DDM mode, which provides a longer delay DDM measurement with an extended shorter delay window. The analysis examined noise floor levels averaged over three separate shorter delay time intervals and computed the 1-sigma variation among the three groups with respect to the mean over the entire noise delay time window. The resulting error statistics are summarized in Table II and show maximum fluctuations of less than 0.3 dB.

Notably, the observed fluctuations in the noise floor prevented the implementation of the open ocean calibration, as described in [4]. The open ocean calibration was meant to monitor and update the instrument hardware look-up tables on orbit and correct for the effects of instrument aging. The strategy for these on-orbit hardware corrections is being redesigned with details available in [10].

TABLE II

NOISE FLOOR UNCERTAINTY INTRODUCED INTO THE CYGNSS LEVEL 1 CALIBRATION DUE TO NON-COMMON MODE NOISE FLOOR EFFECTS

Parameter	Starboard	Port
1-Sigma Uncertainty	0.018 dB	0.020 dB
Maximum Uncertainty	0.26 dB	0.28 dB
Uncertainty Greater than 0.1 dB	1.5 percent	1.6 percent

VI. INVESTIGATING NOISE LEVEL FLUCTUATIONS VERSUS LOCAL TIME

Previous studies have observed the presence of sun noise in L-band measurements [11]. Results were analyzed for both the Starboard and Port antennas and during both Summer (June) and Winter (December) months. There were some visible hourly noise trends in the data with respect to local time, but we found no clear correlation between increased antenna noise and local daylight hour in the CYGNSS data.

We suspect that the noise fluctuations due to other GNSS and particularly SBAS reflections may be greater than the detectable sun-induced noise fluctuations. To observe any existing sun noise effect in the data, it would require a detailed SBAS noise correction, which we will be explored in greater detail in future work.

VII. CONCLUSION

This letter analyzes the geographic distribution of noise power in CYGNSS data. The distribution reveals a regional correlation of noise power level with the CYGNSS observatory receive antenna gain toward specular reflection points of multiple SBAS satellites. First-order analysis and spatial noise power patterns reveal that reflections from the WAAS SBAS satellites are particularly evident. It is found that while the SBAS reflections impact the CYGNSS noise floor levels, the specular reflections of other GNSS transmitters do not have a noticeable impact. Finally, analysis is performed verifying that the additional noise is the common mode between signal + noise and noise-only portions of the DDM, and the resulting error to CYGNSS calibration is negligible.

REFERENCES

[1] S. Gleason and D. Gebre-Egziabher Ed., *GNSS Applications and Methods*. Norwood, MA, USA: Artech House, 2009.

[2] P. Misra and P. Enge, *Global Positioning System: Signals, Measurements, and Performance*. Lincoln, MA, USA: Ganga Jamuna Press, 2001.

[3] C. S. Ruf, "New ocean winds satellite mission to probe hurricanes and tropical convection," *Bull. Amer. Meteorological Soc.*, vol. 97, no. 3, pp. 385–395, 2016. doi: 10.1175/BAMS-D-14-00218.1.

[4] S. Gleason, C. S. Ruf, M. P. Clarizia, and A. J. O'Brie, "Calibration and unwrapping of the normalized scattering cross section for the cyclone global navigation satellite system," *IEEE Trans. Geosci. Remote Sens.*, vol. 54, no. 5, pp. 2495–2509, May 2016. doi: 10.1109/TGRS.2015.2502245.

[5] G. Foti, C. Gommenginger, M. Unwin, P. Jales, J. Tye, and J. Roselló, "An assessment of non-geophysical effects in spaceborne GNSS Reflectometry data from the UK TechDemoSat-1 mission," *IEEE J. Sel. Topics Appl. Earth Observ. Remote Sens.*, vol. 10, no. 7, pp. 3418–3429, Jul. 2017.

[6] V. U. Zavorotny and A. G. Voronovich, "Scattering of GPS signals from the ocean with wind remote sensing application," *IEEE Trans. Geosci. Remote Sens.*, vol. 38, no. 2, pp. 951–964, Mar. 2000.

[7] E. Kahr, O. Montenbruck, and K. O'Keefe, "An analysis of SBAS signal reception in space," *Navigat. J. Inst. Navigat.*, vol. 63, no. 3, pp. 321–333, Sep. 2016.

This article has been accepted for inclusion in a future issue of this journal. Content is final as presented, with the exception of pagination.

[8] T. Wang, C. Ruf, B. Block, and D. McKague, "Characterization of the transmit power and antenna pattern of the GPS constellation for the CYGNSS mission," in *Proc. IGARSS*, Jul. 2018, pp. 4011–4014.

[9] C. Bussy-Virat, J. Getchius, and A. Ridley, "The spacecraft orbital characterization kit and its applications to the CYGNSS mission," in *Proc. Space Flight Mech. Meeting*, 2018. doi: 10.2514/6.2018-1973.

[10] S. Gleason, *CYGNSS Algorithm Theoretical Basis Document Level 1A DDM Calibration*, document 148-0136, University of Michigan, Ann Arbor, MI, USA, 2018.

[11] N. Reul, J. Tenerelli, B. Chapron, and P. Waldteufel, "Modeling sun glitter at L-band for sea surface salinity remote sensing with SMOS," *IEEE Trans. Geosci. Remote Sens.*, vol. 45, no. 7, pp. 2073–2087, Jul. 2007.